MICROBUBBLES AS ULTRASOUND CONTRAST AGENTS

Thomas J. Matula
Applied Physics Laboratory, University of Washington
Seattle, Washington 98105

and

Hong Chen
Department of Biomedical Engineering, Columbia University
New York, New York 10027

Introduction

"The future of healthcare is bubbles."

The future of healthcare is bubbles. That may be an overstatement, but micron-sized bubbles (called microbubbles) play an important role in diagnostic imaging. Current research is exploring how microbubbles can be used for molecular imaging and targeted drug delivery. The bubbles act as very good ultrasound scatterers, and because they oscillate upon ultrasound exposure, they can also do (therapeutic) work on the surrounding tissue (e.g., breaking blood clots or opening up the blood-brain barrier). Current research with microbubbles has focused on two main areas—developing new ultrasound pulse sequences to improve the contrast/noise ratio, and developing specialized microbubbles for molecular imaging and therapy. This article discusses aspects of microbubbles and their dynamics in actual blood vessels.

Before delving into microbubbles, we begin with a question. Why bother with ultrasound as a molecular imaging/therapy modality? Molecular imaging is already being developed for other imaging modalities such as Positron Emission Tomography (PET) and Magnetic Resonance Imaging (MRI). At first glance, ultrasound seems very limited in terms of its ability to image molecules and molecular markers. The answer is simple, and perhaps game-changing—all molecular imaging modalities require some sort of contrast agent. Gadolinium-based agents are examples of MR contrast agents; fluorine 18 is an example for PET. With the addition of ultrasound contrast agents like microbubbles that are targeted to specific antigens, ultrasound too has the potential of being able to image disease proteins at the molecular level. Ultrasound has the added benefits of being low cost, non-invasive, highly portable, uses no radiation, and allows for real time imaging (ultrasound portability is illustrated in Fig. 1). Microbubbles can also be made to grow and collapse at higher pressures, inducing bioeffects such as opening up the endothelium to allow for drug transport across the normally tight cell junctions.

There are several types of ultrasound contrast agents being developed and tested. Figure 2 illustrates some potential formulations. These include perfluorocarbon (PFC) nanodroplets, echogenic liposomes, solid nanoparticles, polylactic acid (PLA) nanobubbles, and microbubbles. An excellent review is provided in the references.[1] This article focuses on microbubbles.

Microbubbles were originally developed to help improve diagnostic ultrasound imaging. The idea is that bubbles, being very good scatterers of ultrasound, would dramatically improve ultrasound image contrast. The first generation bubbles weren't very good—they dissolved too quickly, making it difficult to obtain good images. To improve their stability, today's microbubbles are filled with heavier gases of lower solubility and diffusivity (such as fluorocarbons or sulfur hexafluoride). Microbubbles are also coated with a shell to help slow the diffusion process (shell materials include human serum albumin, lipids, or polymers). Both shell and gas must be biocompatible.

Characterizing shell parameters

The equation that describes a bubble's response to incident ultrasound is a variation of the Rayleigh-Plesset equation. It is a highly nonlinear equation with the addition of parameters that describe the viscoelastic shell. The shell is a very important property of a microbubble—it provides stability to the microbubble as it circulates throughout the vasculature; it adds stiffness to the microbubble, affecting the

Fig. 1. From left to right: PET-CT imaging system, "portable" MRI imaging system, and a cell phone-sized handheld ultrasound imaging system. The portability and low cost features of ultrasound may significantly reduce healthcare costs. (Public domain images).

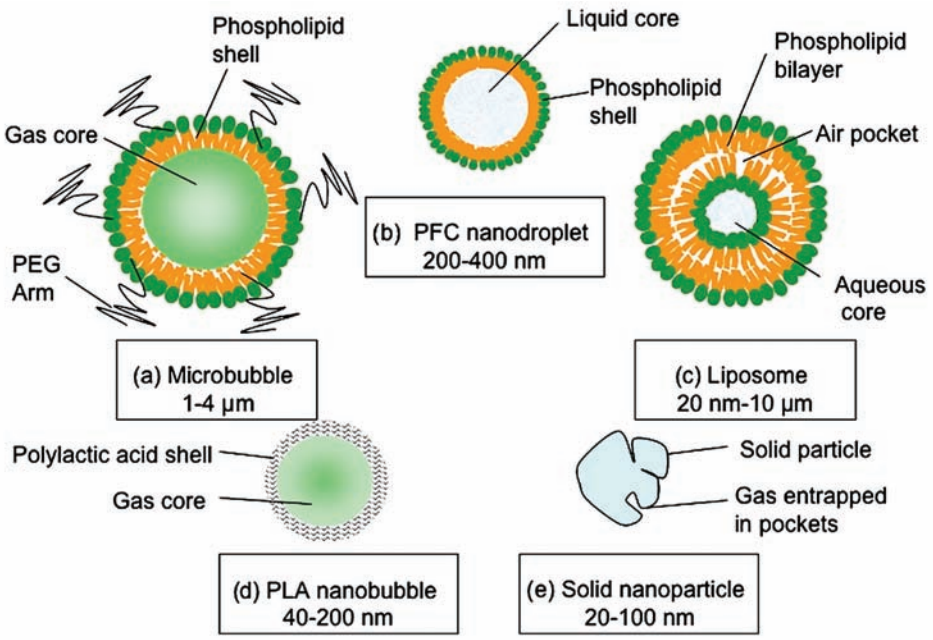

Fig. 2. Various formulations of ultrasound contrast agents.[1] The focus of this article is on microbubbles, gas-filled bubbles with a stabilizing shell. Microbubbles are vascular contrast agents, while nano-formulations may be more suited for extravascular applications. (Reprinted with permission from Elsevier).

bubble's response to ultrasound, and it is the backbone for conjugating ligands for site specific targeting applications.

There are a few bubble dynamics models that incorporate shell properties,[2-7] and a few models have been tested against experimental data.[8-11] All models currently being used are variations of a simple linear viscoelastic shell model. One model that appears to work well for lipid-coated microbubbles is the "Marmottant" model.[5] It is essentially given by:

$$\rho_L\left(R\ddot{R}+\frac{3}{2}\dot{R}^2\right)=\left(P_0+\frac{2\sigma_0}{R_0}\right)\left(\frac{R}{R_0}\right)^{-3\gamma} -\left(P_0+\frac{2\sigma}{R}+\frac{4\mu\dot{R}}{R}+\frac{4\kappa_S\dot{R}}{R^2}+P_a\right) \quad (1)$$

The right hand side is the difference between the interior and exterior pressures. ρ_L is the fluid density, R is the microbubble radius, R_0 is the ambient or initial radius, the dots above the variables denote derivative with respect to time, P_0 is the ambient pressure, P_a is the applied acoustic pressure (e.g., from an ultrasound machine), μ is the liquid viscosity, κ_S is the surface (2-D) dilatational viscosity of the shell, σ_0 is the surface tension between air and water, and σ is a variable surface tension that depends on microbubble size.

The idea of a variable surface tension comes about from considering a fixed monolayer coating (the shell), and how that changes when the microbubble size varies. The coating itself reduces the surface tension. However, during a negative tensile phase of the ultrasound pulse, the microbubble grows. The number of molecules on the microbubble surface is fixed, thus if the bubble grows large enough, gaps between the molecules will increase until the surface tension essentially reaches its air/water value.[12] This is called the "ruptured" state, as though the shell was ruptured and the underlying air/water interface was completely exposed. Conversely, as the bubble shrinks during the compressive phase, the molecular density increases until the molecules "buckle." At this stage the surface tension is minimized, and is set to 0 in the model. In between the buckled and ruptured state, the surface tension is assumed to vary elastically with microbubble size. Thus, the surface tension can be modeled as[5]

$$\sigma(R)=\begin{cases}0 & \text{if } R\le R_{\text{buckling}}\\ \chi\left(\frac{R^2}{R_{\text{buckling}}^2}-1\right) & \text{if } R_{\text{buckling}}\le R\le R_{\text{break-up}}\\ \sigma_0 & \text{if ruptured and } R\ge R_{\text{ruptured}}\end{cases} \quad (2)$$

where χ is an elasticity coefficient for the shell (the viscous contribution κ_S is explicitly given in the bubble dynamics equation above).

An example of how well this model works is illustrated in Fig. 3. For this data, light scattering was used to record the radial dynamics of a microbubble subjected to an ultrasound pulse of 308 kPa near 1 MHz insonation frequency. The model matches the radial oscillations fairly well. There is

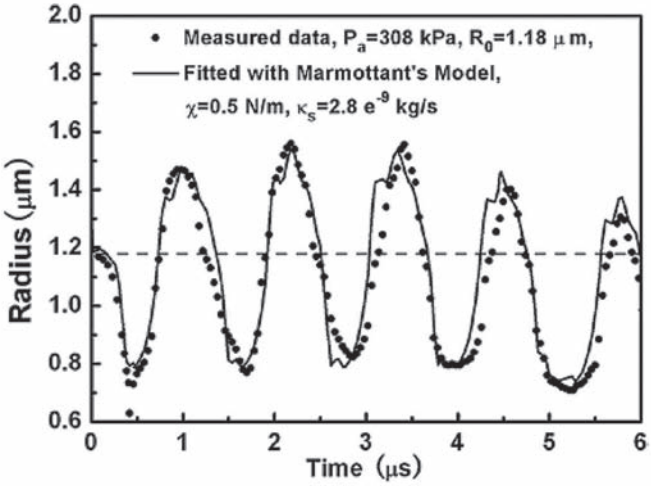

Fig. 3. This data comes from a Definity microbubble. It fit to the Marmottant model. The bubble was driven at 1 MHz with an acoustic pressure of Pa = 308 kPa. The best-fit shell parameters are χ= 0.5 N/m and κ_s = 2.8 x 10^{-9} kg/s, with R_0=1.18 μm. The dashed line indicates the position of R_0. Reprinted[10] with permission.

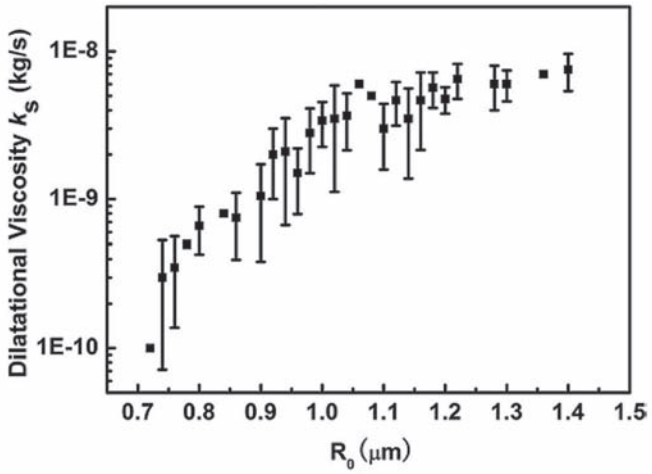

Fig. 4. The dilatational viscosity for Definity microbubbles is shown as a function of ambient microbubble size (radius). Reprinted.[10]

even the hint that the microbubble spent more time compressed than under expansion. This has been termed "compression only" behavior.[13-14]

The dilatational viscosity also apparently depends on ambient microbubble size R_0. Figure 4 illustrates how the experimentally-determined viscosity increases with R_0, at least for smaller microbubbles. The plot suggests that as the microbubble size increases beyond about 3 μm diameter, the viscosity parameter reaches an equilibrium value nearing about 1 x 10^{-8} kg/s. Whether or not the real viscosity depends on microbubble size as shown in the figure is unknown, as the shell model itself may not be very accurate. For example, if a linearized version of the Marmottant equation is used, the elasticity parameter also is a function of microbubble size.[9] However, if the nonlinear version is used, the elasticity parameter appears to be constant (0.7 and 0.5 N/m, for Definity and Sonovue, respectively).[10]

Optimizing diagnostic ultrasound pulse sequences for contrast imaging can be complicated if the shell parameters are functions of microbubble size. Consider that a 1-ml vial might contain over 10^8 microbubbles, with a size distribution ranging from under 1 μm to over 10 μm in diameter. Because they are relatively large, they are constrained to the vasculature (this makes them good blood flow tracers). However, as they pass through the lung capillary bed, many of the microbubbles are destroyed. Some are held up because they're too large to pass through the pulmonary circulation. Some break (dissolve) naturally as the shell may not evenly coat the microbubble. The injection process itself may lead to rupture of many microbubbles. As many as half the original number might be destroyed during the first pass through the circulation. Because of these processes, the microbubble size distribution *in vivo* is unknown. This makes it difficult to tune an ultrasound system for optimizing microbubble signals, as microbubbles have sharp resonances. Some researchers are using microfluidics to generate monodisperse microbubbles,[15-17] but a lack of stability and large size limit their clinical use at this time.

Mechanisms of vascular bioeffects

How does an oscillating microbubble generate a bioeffect? In 1917, Rayleigh noted that a collapsing bubble can generate sufficient pressures to damage nearby surfaces.[18] For a bubble collapsing near a rigid boundary, a liquid jet can form that penetrates through the bubble and toward the boundary. Such jets have long been considered a potential source of damage to nearby surfaces.[19] While early studies of bubble-induced damage were motivated by cavitation damage to ship propellers,[20] medical ultrasound has brought focus to interactions between microbubbles and viscoelastic tissues. Observations of bubbles near lipid membranes,[21] biological cells,[22] or viscoelastic gels[23] indicate that a nearby compliant boundary can be deformed by pushing and pulling forces associated with volumetric bubble oscillations. However, most studies use more rigid boundaries. For example, one study using cells mounted on a rigid substrate suggested that cell membranes are disrupted by the impingement of liquid jets directed at the cells.[22] These types of *in vitro* studies do not directly address the clinical environment in which microbubbles are constrained within viscoelastic blood vessels. In addition to possessing unknown viscoelastic properties, blood vessels also impose a volumetric confinement on bubble oscillations. Constrained within blood vessels, microbubbles excited by ultrasound not only can rupture the vessel,[24] but also can affect the vascular endothelium; there is hope that the latter effect can be exploited to modify vessel permeability to enhance local drug or gene delivery.[21,25-26]

Accordingly, numerical simulations[27-30] and experiments[31-32] have sought to elucidate how bubbles and vessels interact. Based on prior work, vascular rupture in ultrasound applications has been attributed to either liquid jet impingement or vessel distention due to "pushing" forces.[31-33] Here, we used ultra-high speed photomicrography to visualize directly transient interactions between ultrasound-activated microbubbles and blood vessels within *ex vivo* tissue. Both

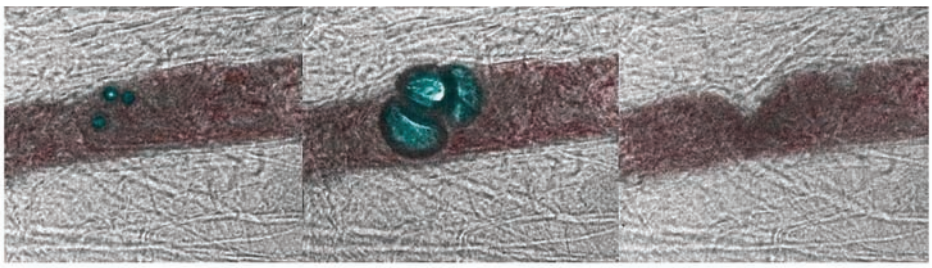

Fig. 5. A group of bubbles distends the vessel wall (middle) during the tensile portion of the sound wave; subsequent invagination (right) appears localized and markedly larger than the distention. Time stamps are, from left to right, 1.3, 1.6, and 3.4 μs after arrival of a 2-cycle ultrasound pulse of amplitude 6.4 MPa. Vessel diameter is approximately 46 μm. Images were colored

bubble oscillations and vessel displacements were observed on microsecond time scales.

For these experiments, approved by the University of Washington institutional animal care and use committee (IACUC), a rat mesentery was selected as the animal tissue model because it contains thin and transparent regions, allowing easy observations of its microvasculature under light microscopy. Experiments were conducted on vessels ranging from about 10-100 μm in diameter. These included arterioles, venules and capillaries. The confinement imposed by these vessels and surrounding tissue did not prevent bubbles from undergoing large volumetric oscillations that included inertial collapses. In turn, vessels deformed on the same microsecond time scale as bubble oscillations. A typical observation of bubble dynamics is illustrated in Fig. 5. The tensile portion of the sound wave leads to microbubble growth, causing distention of the nearby vessel wall. The subsequent invagination of the vessel wall follows inertial bubble collapse. In this and most other cases, invagination appears more localized, suggesting higher stresses and strains than those resulting from distention. We could hypothesize, based on these findings, that invagination may be a principal mechanism for bioeffects, at least in these types of vessels.[34] Other vessels such as arteries are much stiffer than these vessels, and may not respond in the same manner. Still, most of the available evidence from *in vivo* studies indicates that vessel permeabilization effects occur principally in the microcirculation—that is, arterioles, venules and capillaries.

To quantify the observed vessel displacements, radial displacements of the point on the vessel wall closest to the center of the bubble were measured, and results obtained from four representative high-speed image sequences[34] are plotted in Fig. 6. In each of these cases, distention was small relative to invagination. Moreover, vessel walls behaved similarly in that the average inward wall speed was around 9 m/s over the time range from 1.5–2.5 μs. Achieving such a velocity over such a short time scale implies that this response was forced rather than evoked. In addition, vessels achieved their maximum invaginations after the ultrasound pulse had passed and bubble motions had mostly ceased.

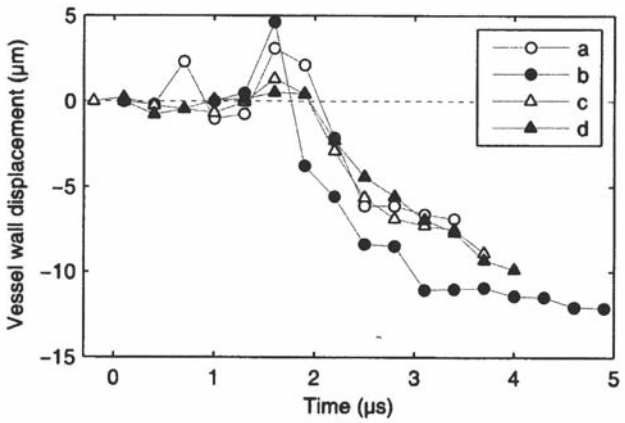

Fig. 6. Measurements of radial displacements of the vessel wall at the point closest to the bubble for four different experiments. Each marker denotes a measurement from a single image frame. Deflections toward the lumen were defined to be negative. For each of these sequences, vessel invagination exceeded distention by a significant margin. The observed invaginations occurred after bubbles collapsed (at about 2 μs in the plot) and persisted even after bubbles rebounded.[34]

Although invagination is often greater than distension, we have also seen evidence that distention can be greater than invagination in small microvessels with high insonation pressures. The image sequence shown in Fig. 7 suggests that for small microvessels at high pressures, distention might be significant enough to rupture the vessel wall. However, this appears to be limited to small vessels under high pressures, in which the bubble expands significantly beyond the original diameters of the blood vessels.

We mentioned above that jetting is thought to be the other principal mechanism for some of the observed bioeffects. We too observed clear evidence of jetting microbubbles in these vessels. Figure 8 illustrates one such observation. However, the jet was directed *away* from the nearby vessel wall, not towards it. In fact, in all of our data sets (over 20) in which jets can be clearly resolved, *all* of them were directed away from the nearest boundary.[35] In Fig. 8 the microbubble

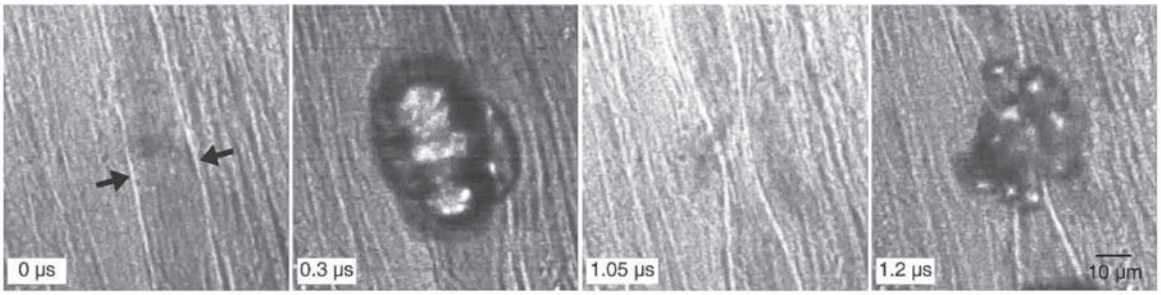

Fig. 7. A high-speed image sequence that shows expansion, collapse and re-expansion of a bubble cluster, accompanied by the observation of vessel distention and invagination. Vessel diameter =17 m; ultrasound peak negative pressure = 7 MPa. The bubble fragments outside the vessel at 1.2 μs indicate the vessel was ruptured.

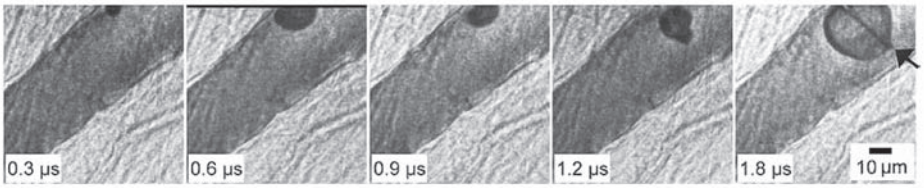

Fig. 8. Microjet formed in a 48 μm diameter microvessel under a peak negative pressure of 3 MPa.[35] *The scale bar represents 10 mm.*

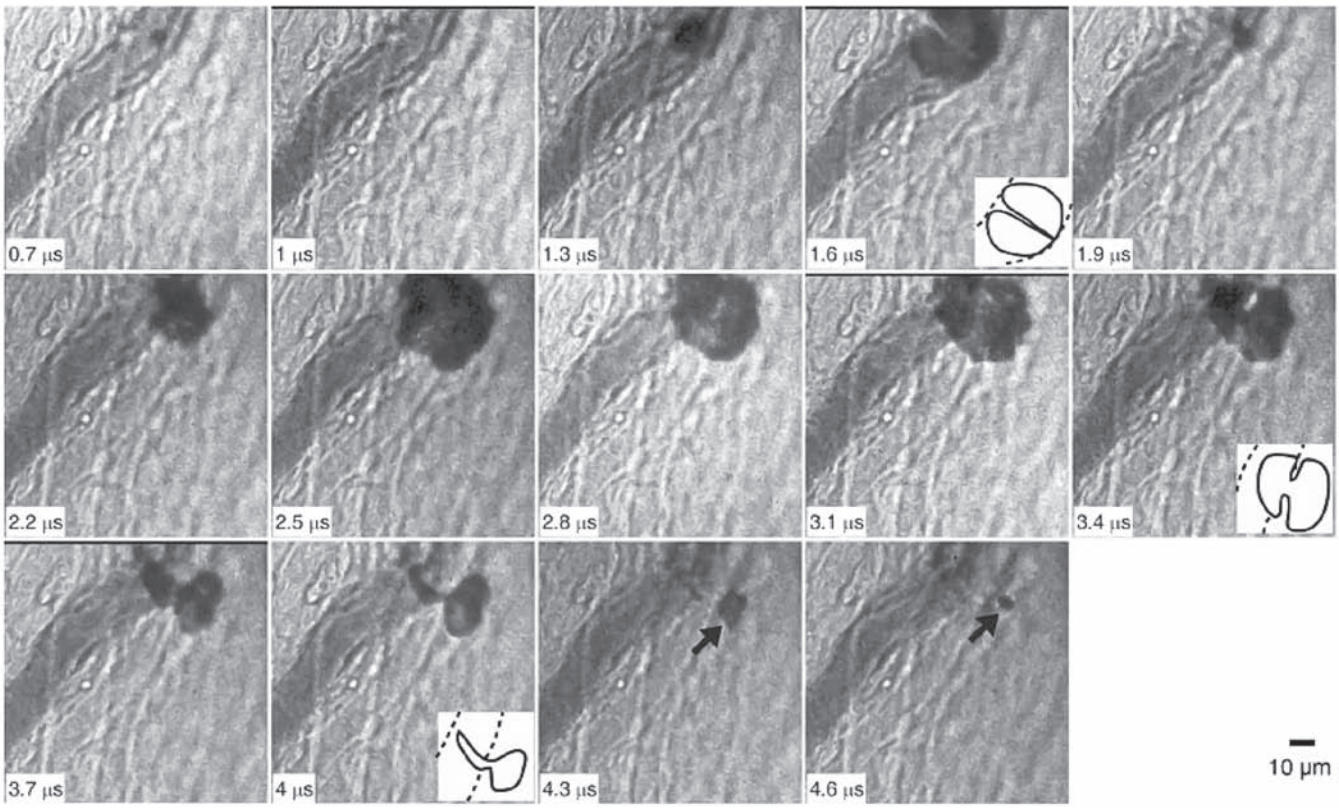

Fig. 9. Vascular rupture involving a liquid jet. Peak negative pressure = 4 MPa. Vessel diameter = 15 µm. In frame 4, a liquid jet is seen directed toward the right side vessel wall. In frame 12, the bubble appears as a mushroom shape with its stem stretching through the vessel wall. Sketches of the bubble in these characteristic frames are marked with the bubble in solid lines and vessel in dashed lines. In the last frame, the collapsed bubble (arrow) was observed in the interstitial space outside the vessel.

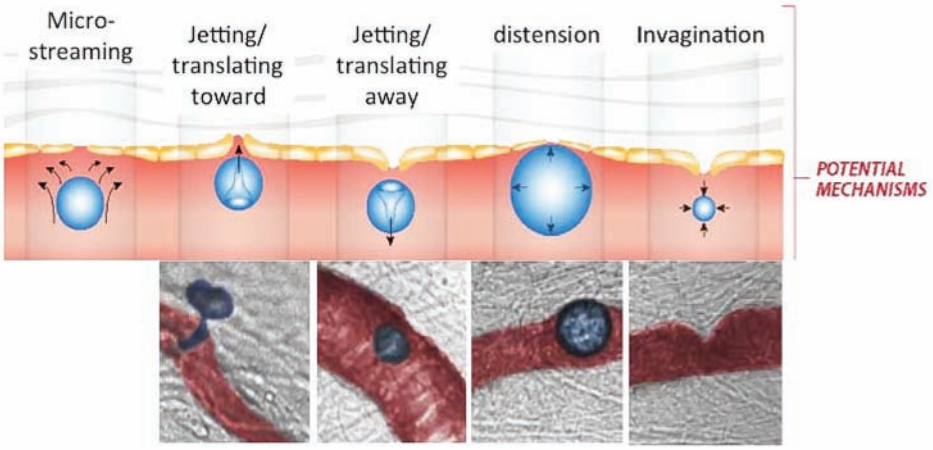

Fig. 10. Illustration of potential mechanisms for microbubble-induced bioeffects.

expanded against the left vessel wall (0.3 and 0.6 µs) and then contracted (0.9 µs). It re-expanded at 1.2 µs. During further re-expansion, a microjet is seen to penetrate through the interior of the microbubble (1.8 µs). The direction of the microjet was away from the left vessel wall. The length of the (identifiable) microjet was about 38 µm, which is smaller than the vessel diameter. Consequently, the microjet does not appear to impact the vessel wall. Additionally, if we assume that the microjet started to form at 0.9 µs, an average speed of 42 m/s can be estimated between 0.9 and 1.8 µs. This estimate is probably a lower bound, as the microjet may have started to form towards the end of collapse or early in the rebound. The lower bound water hammer pressure generated by this jet was about 63 MPa.

One can ask, "If the vessel were smaller, would the jet impact the opposite wall?" The answer is "yes!" Figure 9 shows how a microbubble jet can impact and rupture a vessel wall. The jet is seen in the fourth frame (1.6 µs), and the re-expanding microbubble is found in the tissue beyond the vessel boundary (last 3 frames). Our conclusion is that a microbubble in a compliant microvessel can jet, that the jet is directed away from the nearest vessel wall, and it can impact the distal vessel wall if the vessel is smaller than the length of the jet.

Our observations suggest that bioeffects can occur through distension, invagination, or jetting. We hypothesize that invagination (like that shown in Fig. 5) is the principal mechanism for larger microvessels, while jetting (e.g., Figs. 8-9) and distension (e.g., Fig. 7) become important for smaller microvessels. The potential and observed bioeffect mechanisms are assembled in Fig. 10. Understanding and optimizing cavitation for specific bioeffects should lead to improved diagnosis and treatment at reduced costs. The future of healthcare is bubbles! AT

Acknowledgments

This work could not have been completed without contributions from Mike Bailey, Andrew Brayman, Wayne Kreider, Frank Starr, and Juan Tu. Funding from NIH (NIBIB, NIDDK, and NIAMS) is gratefully acknowledged.

References

1 N. Deshpande, A. Needles, and J.K. Willmann, "Molecular ultrasound imaging: current status and future directions," Clinical Radiol. **65**(7), 567–81, 3144865 (2010).

2 D. Chatterjee and K. Sarkar, "A Newtonian rheological model for the interface of microbubble contrast agents," Ultrasound in Med. and Biol. **29**(12), 1749–1757 (2003).

3 A. A. Doinikov, J. F. Haac, and P. A. Dayton, "Modeling of nonlinear viscous stress in encapsulating shells of lipid-coated contrast agent microbubbles," Ultrasonics **49**(2), 269–275 (2009).

4 N. de Jong, R. Cornet, and C. T. Lancee, "Higher harmonics of vibrating gas-filled microspheres. Part one: Simulation," Ultrasonics **32**, 447 (1994).

5 P. Marmottant, S. van der Meer, M. Emmer, M. Versluis, N. de Jong, S. Hilgenfeldt, and D. Lohse, "A model for large amplitude oscillations of coated bubbles accounting for buckling and rupture," J. Acoust. Soc. Am. **118**(6), 3499–3505 (2005).

6 C. C. Church, "The effects of an elastic solid surface layer on the radial pulsations of gas bubbles," J. Acoust. Soc. Am. **97**,1510 (1995).

7 W. Shao and W. Chen, "The dynamics of the aspheric encapsulated bubble," J. Acoust. Soc. Am. **133**(1), 119–126 (2013).

8 K. Sarkar, W. T. Shi, D. Chatterjee, and F. Forsberg, "Characterization of ultrasound contrast microbubbles using in vitro experiments and viscous and viscoelastic interface models for encapsulation," J. Acoust. Soc. Am. **118**(1), 539–550 (2005).

9 J. Tu, J. F. Guan, Y. Y. Qiu, and T. J. Matula, "Estimating the shell parameters of SonoVue (R) microbubbles using light scattering," J. Acoust. Soc. Am. **126**(6), 2954–2962 (2009).

10 J. Tu, J. Swalwell, D. Giraud, W. Cui, W. Chen, and T. Matula, "Microbubble sizing and shell characterization using flow cytometry," IEEE Trans. Ultrasonics, Ferroelectrics, and Frequency Control **58**(5), 955–963 (2011).

11 N. de Jong, R. Cornet, and C. T. Lancee, "Higher harmonics of vibrating gas-filled microspheres. Part two: Measurements," Ultrasonics **32**, 455 (1994).

12 F. Graner, S. Perez-Oyarzun, A. Saint-Jalmes, C. Flament, and F. Gallet, "Phospholipidic monolayers on formamide," J. Phys. **II 5**, 313 (1995).

13 N. de Jong, M. Emmer, C. T. Chin, A. Bouakaz, F. Mastik, D. Lohse, and M. Versluis, " 'Compression-only' behavior of phospholipid-coated contrast bubbles," Ultrasound in Med. and Biology **33**(4), 653–656 (2007).

14 J. Sijl, M. Overvelde, B. Dollet, V. Garbin, N. de Jong, D. Lohse, and M. Versluis, " 'Compression-only' behavior: A second-order nonlinear response of ultrasound contrast agent microbubbles," J. Acoust. Soc. Am. **129**(4), 1729–1739 (2011).

15 P. Garstecki, I. Gitlin, W. DiLuzio, G. M. Whitesides, E. Kumacheva, and H. A. Stone, "Formation of monodisperse bubbles in a microfluidic flow-focusing device," Appl. Phys. Lett. **85**(13), 2649–2651 (2004).

16 K. Hettiarachchi, E. Talu, M. L. Longo, P. A. Dayton, and A. P. Lee, "On-chip generation of microbubbles as a practical technology for manufacturing contrast agents for ultrasonic imaging," Lab on a Chip **7**(4), 463–468 (2007).

17 Y. Gong, M. Cabodi, and T. Porter, "Relationship between size and frequency dependent attenuation of monodisperse populations of lipid coated microbubbles," Bubble Sci., Eng. & Technol. **2**(2), 41–47 (2010).

18 L. Rayleigh, "On the pressure developed in a liquid during the collapse of a spherical cavity," Philos. Mag. **34**, 94 (1917).

19 T. B. Benjamin and A. T. Ellis, "The collapse of cavitation bubbles and the pressures thereby produced against solid boundaries," Philosophical Trans. of the Royal Soc. of London. Series A, Mathematical and Physical Sciences **260**(1110), 221–240 (1966).

20 J. R. Blake and D. C. Gibson, "Cavitation bubbles near boundaries," Ann. Rev. Fluid Mech. **19**(1), 99–123 (1987).

21 P. Marmottant and S. Hilgenfeldt, "Controlled vesicle deformation and lysis by single oscillating bubbles," Nature **423**(6936), 153–156 (2003).

22 P. Prentice, A. Cuschierp, K. Dholakia, M. Prausnitz, and P. Campbell, "Membrane disruption by optically controlled microbubble cavitation," Nature Phys. **1**(2), 107–110 (2005).

23 E. A. Brujan, K. Nahen, P. Schmidt, and A. Vogel, "Dynamics of laser-induced cavitation bubbles near elastic boundaries: Influence of the elastic modulus," J. Fluid Mech. **433**, 283–314 (2001).

24 D. Miller, M. A. Averkiou, A. A. Brayman, E. C. Everbach, C. K. Holland, J. H. Wible, Jr., and J. Wu, "Bioeffects considerations for diagnostic ultrasound contrast agents," J. Ultrasound in Med. and Biology **27**(4), 633–636 (2008).

25 Z. P. Shen, A. A. Brayman, L. Chen, and C. H. Miao, "Ultrasound with microbubbles enhances gene expression of plasmid DNA in the liver via intraportal delivery," Gene Therapy **15**(16), 1147–1155 (2008).

[26] K. Ferrara, R. Pollard, and M. Borden, "Ultrasound microbubble contrast agents: Fundamentals and application to gene and drug delivery," Ann. Rev. Biomed. Eng. **9**(1), 415–447 (2007).
[27] S. Qin and K. W. Ferrara, "Acoustic response of compliable microvessels containing ultrasound contrast agents," Phys. in Med. and Biol. **51**(20), 5065 (2006).
[28] J. B. Freund, "Suppression of shocked-bubble expansion due to tissue confinement with application to shock-wave lithotripsy," J. Acoust. Soc. Am. **123**(5), 2867–2874 (2008).
[29] H. Miao, S. M. Gracewski, and D. Dalecki, "Ultrasonic excitation of a bubble inside a deformable tube: Implications for ultrasonically induced hemorrhage," J. Acoust. Soc. Am. **124**(4), 2374–2384 (2008).
[30] T. Hay, Y. Ilinskii, E. Zabolotskaya, and M. Hamilton, "Model for the dynamics of a pherical bubble undergoing small shape oscillations between parallel soft elastic layers," J. Acoust. Soc. Am., **in press** (2013).
[31] P. Zhong, Y. F. Zhou, and S. L. Zhu, "Dynamics of bubble oscillation in constrained media and mechanisms of vessel rupture in SWL," Ultrasound in Med. and Biol. **27**, 119–134 (2001).
[32] C. F. Caskey, S. M. Stieger, S. Qin, P. A. Dayton, and K. W. Ferrara, "Direct observations of ultrasound microbubble contrast agent interaction with the microvessel wall," J. Acoust. Soc. Am. **122**, 1191–200 (2007).
[33] S. P. Qin, C. F. Caskey, and K. W. Ferrara, "Ultrasound contrast microbubbles in imaging and therapy: Physical principles and engineering," Phys. in Med. & Biol. **54**(6), R27–R57 (2009).
[34] H. Chen, W. Kreider, A. A. Brayman, M. R. Bailey, and T. J. Matula, "Blood vessel deformations on microsecond time scales by ultrasonic cavitation," Phys. Rev. Lett. **106**(3), 034301, 3087441 (2011).
[35] H. Chen, A. A. Brayman, W. Kreider, M. R. Bailey, and T. J. Matula, "Observations of translation and jetting of ultrasound-activated microbubbles in mesenteric microvessels," Ultrasound in Med. and Biol. **37**, 2139–2148, 22036639 (2011).

Thomas J. Matula earned a Ph.D. degree in physics at Washington State University, Pullman, Washington. He then moved to the Applied Physics Laboratory (APL) in Seattle, Washington, to work on a variety of sonoluminescence and sonochemistry projects. These led to honors from the Department of Defense (Young Scientist and Engineer Award), and the Presidential Early Career Award. His current research interests include ultrasound contrast agents for molecular imaging and therapy, shock wave therapy, and applications of ultrasound to industrial problems. Dr. Matula is currently the Director of the Center for Medical and Industrial Ultrasound (CIMU). He is also the Executive Director of the Center for Ultrasound-Based Molecular Imaging and Therapy (UWAMIT), dedicated to the commercialization of ultrasound-based technologies.

Hong Chen received B.E. and M.E. degrees in Biomedical Engineering from Xi'an Jiaotong University in 2003 and 2006, respectively. She joined the Center for Industrial and Medical Ultrasound at the University of Washington in 2006 for her Ph.D. study. Her thesis focused on understanding the mechanisms by which ultrasound contrast agent microbubbles cause bioeffects to blood vessels. After graduation in 2011, she joined the School of Medicine at the University of Washington as a senior fellow, working on ultrasound enhanced drug delivery to tumors. She then joined the Ultrasound Elasticity Imaging Laboratory at Columbia University in 2012 as a postdoctoral research scientist. Her research now involves working on opening the blood-brain barrier using focused ultrasound.